

Cite this: *Soft Matter*, 2011, **7**, 7366

www.rsc.org/softmatter

PAPER

# Scale-dependent diffusion of spheres in solutions of flexible and rigid polymers: mean square displacement and autocorrelation function for FCS and DLS measurements

Anna Ochab-Marcinek<sup>a</sup> and Robert Hołyst<sup>\*ab</sup>

Received 10th February 2011, Accepted 4th May 2011

DOI: 10.1039/c1sm05217a

We present a theoretical description of diffusion of a sphere in polymer solution. The depletion layer around the sphere affects its motion and leads to scale-dependent diffusion. We propose the model of walking confined diffusion. Although it is different from anomalous diffusion, we show that the experimental data generated by this process may have features characteristic of anomalous diffusion. We give analytical formulas for the autocorrelation functions describing this type of motion in: i) dynamic light scattering experiments and ii) fluorescence correlation spectroscopy experiments. We compare our results to existing experimental data for polyethylene oxide, fd-virus, and F-actin solutions.

## 1 Introduction

A sphere immersed in a solution of non-adsorbing polymer is surrounded by a layer depleted of polymer chains.<sup>1,2</sup> Due to the changes of configurational entropy of polymer chains,<sup>3</sup> the monomer concentration gradually decreases as we approach the surface of the sphere from the bulk of the polymer solution. When the polymer is squeezed close to the surface of the sphere, the entropy strongly decreases, and therefore the centers of mass of polymer chains are excluded from the layer in close proximity to the sphere surface. At the overlap polymer concentration, the thickness of the ‘depletion layer’ is comparable to the radius of gyration  $R_g$  of the polymer, and it decreases with increasing polymer concentration.<sup>4</sup>

The presence of the depletion layer has profound consequences for motion of the sphere through the polymer solution. The sphere’s motion is particularly strongly affected when the radius  $R$  of the sphere is comparable to the depletion layer thickness  $a$ . The viscosity of polymer solutions is a stretched exponential function of polymer concentration.<sup>5–7</sup> Since this concentration is non-uniform, the viscosity around the sphere is also non-uniform and it changes by many orders of magnitude from the solvent viscosity close to the surface of the sphere to the macroviscosity of the bulk solution over the distance of the depletion layer thickness *i.e.* tens of nanometres.<sup>8–10</sup> The flow of the solution around the sphere is complicated and slip effects are generated. The Stokes’ resistance force is between the two limiting cases of a pure solvent and a bulk solution. The effective drag force can

be used to compute the diffusion coefficient according to the Stokes–Sutherland–Einstein equation.<sup>7</sup> This method however, does not allow one to directly calculate the autocorrelation functions for diffusion that are measured in typical experiments of dynamic light scattering (DLS) or fluorescence correlation spectroscopy (FCS). In this paper we present a study complementary to those of Dhont, Fan, and Tuinier,<sup>8–10</sup> in which we derive the DLS and FCS autocorrelation functions for diffusion of spheres in polymer solutions, taking into account the presence of the depletion layer. To derive the autocorrelation functions, we approximate the motion of the sphere in the polymer solution as ‘walking confined diffusion’:<sup>11</sup> fast diffusion of the probe inside the depletion layer, *i.e.* at small length scales, and slow diffusion of the probe together with its depletion layer at large length scales. From the autocorrelation functions, an experimentalist can determine i) the thickness of the depletion layer; ii) the diffusion coefficient of the fast diffusion; iii) the diffusion coefficient of the slow diffusion. These experimentally determined parameters can be further analyzed using the viscosity profiles and Stokes resistance force from the theory developed by Dhont, Fan, and Tuinier.<sup>9,10,12</sup>

The diffusion of spheres with a depletion layer should bear some resemblance to the anomalous diffusion, since the diffusion occurring in inhomogeneous medium is scale-dependent. In many papers, anomalous diffusion is observed in systems where strong depletion effects should occur *i.e.* for  $R \sim R_g$ . For example, Weitz *et al.*<sup>13,14</sup> and Kang *et al.*<sup>15</sup> investigated systems which shared a common feature:  $R \sim R_g$ , *e.g.*  $R = 210$  nm in a polyethylene oxide (PEO) solution of a molecular weight of 4 M ( $R_g = 135$  nm). Mason and Weitz<sup>13</sup> assumed that diffusion occurs in a homogeneous medium and described the motion of the probe in terms of anomalous diffusion. We believe that any sign of anomalous diffusion in such systems should be

<sup>a</sup>Institute of Physical Chemistry, Polish Academy of Sciences, ul. Kasprzaka 44/52, 01-224 Warsaw, Poland. E-mail: holyst@ichf.edu.pl

<sup>b</sup>Cardinal Stefan Wyszyński University, WMP-SNŚ, ul. Dewajtis 5, 01-805 Warsaw, Poland

approached with caution and one should consider whether the description in terms of the depletion layer effect might be more appropriate.

The paper is organized as follows: In Section 2 we present the model (Subsection 2.1), then we derive the formulas for the mean square displacement (Subsection 2.2) and discuss the similarities and differences between walking confined diffusion and anomalous diffusion (Subsection 2.3). Next, we derive the diffusion propagator (Subsection 2.4), as well as the DLS and FCS autocorrelation functions for the diffusion with depletion layer (Subsection 2.5). In Section 3 we predict the experimental consequences of the depletion layer effect for a system with parameters typical for a spherical probe diffusing in polyethylene glycol (PEG) solution and discuss the similarity of these predictions to the experimental results described in literature in terms of anomalous diffusion. Subsection 3.1 discusses the behavior of MSD for a probe diffusing with depletion layer; Subsection 3.2 and 3.3 show the typical shapes of DLS and FCS autocorrelation functions for the diffusion with depletion layer; they also discuss how the measured diffusion coefficients would change if one made an attempt of fitting the two-component diffusion or single-component free diffusion autocorrelation functions to the experimental data in which the depletion layer effect is present. In the Section 4 we compare our theory with experimental data for the solutions of PEO, fd viruses and F-actin. Section 5 summarizes our findings.

## 2 Walking confined diffusion as a model of diffusion with depletion layer

### 2.1 The model

We propose a simplistic model of the depletion layer (Fig. 1) as a sphere of a radius  $R_{\text{tot}}$ , diffusively moving with the diffusion coefficient  $D_M$  in the polymer solution. Enclosed in the sphere is a probe of a radius  $R$ , moving with the diffusion coefficient  $D_m$ . The boundaries of the sphere are assumed to be reflecting. We assume that  $D_m \gg D_M$  to ensure that the diffusion of the sphere and the confined diffusion of the probe inside the sphere can be

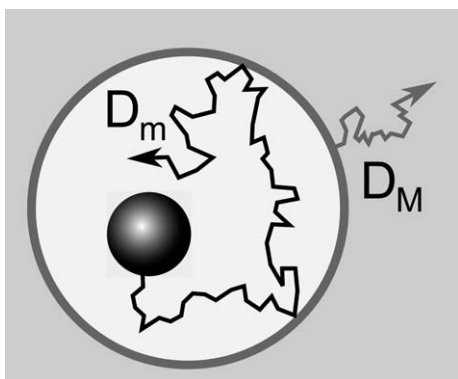


**Fig. 1** Walking confined diffusion as a model of diffusion with depletion layer. The motion of the probe in the medium is split into two independent components: The depletion layer is a sphere of the radius  $R_{\text{tot}}$  that freely diffuses with the coefficient  $D_M$ . Enclosed in the sphere is the probe of the radius  $R$ , diffusing with the coefficient  $D_m \gg D_M$ . The boundaries of the sphere are reflecting.

considered as independent. This type of motion is called ‘walking confined diffusion’.<sup>11</sup>

The model captures the essential features of diffusion with depletion layer: In short time scales, only the fast motion of the probe in the solvent is visible in the form of free diffusion with the microscopic coefficient  $D_m$ . In long time scales, only the slow motion of the sphere together with its depletion layer is visible in the form of free diffusion with the macroscopic coefficient  $D_M$ . In the intermediate time scales, a crossover occurs between those two diffusion regimes.

In the short time scale (the relaxation time of the depletion layer), the microscopic diffusion coefficient  $D_m$  depends on the solvent viscosity and on the hydrodynamic flow profile around the probe. The macroscopic diffusion coefficient of the spherical probe diffusing together with its depletion layer is

$$D_M = \frac{k_B T}{6\pi\eta_M(R+a)}, \quad (1)$$

where  $\eta_M$  is the macroscopic viscosity of the polymer solution (see, however, Holyst *et al.*<sup>7</sup> for scale-dependent viscosity), and  $a = R_{\text{tot}} - R$  is the depletion layer thickness.

In this study, we make the assumptions about the polymer solution that enable us to calculate  $a$  using the literature data<sup>16,17</sup> for PEG-2M, which we will further use to predict the possible experimental results (Section 3). We assume that the polymer solution is dilute, so that  $a$  does not depend on its concentration, and that the solution can be described in the Gaussian limit, *i.e.* as infinitely long and thin polymers. In such a case, the formula of Tuinier<sup>18</sup> applies:

$$a = R \left[ \left( 1 + \frac{6}{\sqrt{\pi}} \frac{R_g}{R} + 3 \left( \frac{R_g}{R} \right)^2 \right)^{1/3} - 1 \right], \quad (2)$$

where  $R_g$  is the radius of gyration of the polymer. However, the diffusion propagator that we derive below uses a generalized depletion layer thickness  $a$ , which can be obtained experimentally or calculated for other cases of polymer solutions.

### 2.2 Mean square displacement for diffusion with depletion layer

Instead of calculating the exact propagator for walking confined diffusion, we adopt the technique used in modelling of anomalous diffusion:<sup>19–23</sup> Since the autocorrelation functions in FCS and DLS depend on the mean square displacement (MSD) of the probe, we construct the propagator of free diffusion with the time-dependent diffusion coefficient  $D(t)$ , which generates the same MSD as the process of walking confined diffusion. Since the diffusive motions of the probe and the sphere are independent and  $\langle \mathbf{r}_m \rangle = \langle \mathbf{r}_M \rangle = 0$ , their mean square displacements are additive. The MSD for the freely diffusing sphere is

$$\langle \mathbf{r}_M^2(t) \rangle = 6D_M t. \quad (3)$$

The MSD for the confined diffusion inside an immobile sphere is<sup>24</sup>

$$\langle \mathbf{r}_m^2(t) \rangle = \frac{6a^2}{5} - 12a^2 \sum_{n=1}^{\infty} \exp \left[ -\beta_{1n}^2 \frac{D_m t}{a^2} \right] \frac{1}{\beta_{1n}^2 (\beta_{1n}^2 - 2)}, \quad (4)$$

where  $\beta_{1n}$  are the (non-zero) zeros of the derivatives of the spherical Bessel function,  $j_1'(\beta_{1n}) = 0$ . The first terms of eqn. (4) are the following:

$$\langle \mathbf{r}_m^2(t) \rangle = \frac{6}{5} a^2 \left( 1 - 0.99 e^{-\frac{4.33 D_m t}{a^2}} - 0.0085 e^{-\frac{35.29 D_m t}{a^2}} - \dots \right) \quad (5)$$

Eqn. (4) can be approximated by

$$\langle \mathbf{r}_m^2(t) \rangle = 6 D_m \tau \left( 1 - e^{-\frac{t}{\tau}} \right), \quad (6)$$

where  $\tau = a^2/5D_m$  is the characteristic equilibration time. The MSD for walking confined diffusion is therefore:

$$\begin{aligned} \langle \mathbf{r}^2(t) \rangle &= \langle \mathbf{r}_m^2(t) \rangle + \langle \mathbf{r}_M^2(t) \rangle \\ &= 6 D_M t + \frac{6}{5} a^2 \left( 1 - e^{-\frac{5 D_m t}{a^2}} \right). \end{aligned} \quad (7)$$

In the long time limit,  $\langle \mathbf{r}_m^2 \rangle$  tends to  $6a^2/5$ , in accordance with eqn. (4). In experiments, the diffusion of probes with depletion layer can be detected as diffusion with a time-dependent diffusion coefficient  $D(t)$ , defined by the relation<sup>19</sup>

$$\langle \mathbf{r}^2(t) \rangle = 2d \int_0^t D(t') dt', \quad (8)$$

where  $d = 3$  is the spatial dimension. Then

$$D(t) = D_M + D_m e^{-\frac{t}{\tau}}. \quad (9)$$

Assuming that  $D_M \ll D_m$ ,  $D(t)$  transitions from  $D_m$  on a short time scale to  $D_M$  on a long time scale. Note that Daumas *et al.*<sup>11</sup> proposed a formula similar to eqn. (7) for MSD in 2-dimensional walking confined diffusion. However, their heuristic derivation was incorrect and it would not give the correct formula (eqn. (7)) in 3 dimensions.

### 2.3 Walking confined diffusion vs. anomalous diffusion

Anomalous diffusion is a process with  $\langle \mathbf{r}^2(t) \rangle \sim t^\alpha$ , where  $\alpha \neq 1$  ( $\alpha$  being the slope of the log-log plot of the MSD, see Fig. 2, inset). Walking confined diffusion is not anomalous diffusion. However, similarly as in the Rouse and the reptation models,<sup>25</sup> the MSD (eqn. (7)) in the walking confined diffusion model can be approximated by  $t^\alpha$  in various time scales.  $\alpha = 1$  in the short ( $t \rightarrow 0$ ) and long time scales ( $t \rightarrow \infty$ ), and  $\alpha < 1$  in the intermediate time scales. For this reason, the experimental data generated by the process of walking confined diffusion can be similar to anomalous diffusion, if the measurement covers the intermediate time scales only. For the crossover time  $t = \tau$ ,

$$\alpha = \frac{D_m + D_M e}{D_m(e-1) + D_M e}, \quad (10)$$

and assuming that  $D_M \ll D_m$ ,

$$\alpha \approx \frac{1}{e-1} \approx 0.6. \quad (11)$$

At a certain time  $t > \tau$  the log-log plot of the MSD has the smallest slope, however the value of  $\alpha$  in this point can be

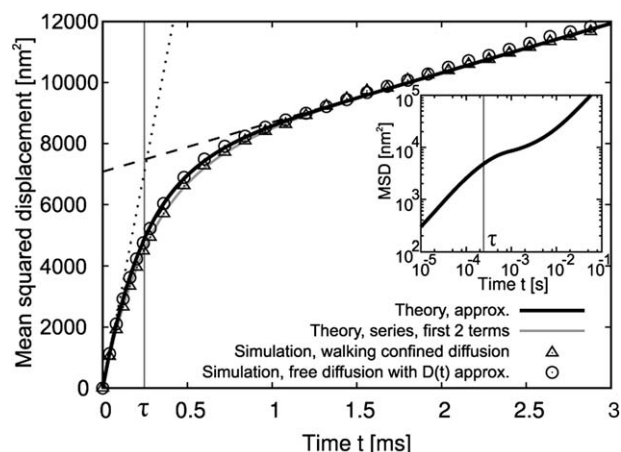


**Fig. 2** Mean square displacement for walking confined diffusion. Black line: the approximate eqn. (6). Gray line: two first terms of the exact eqn. (5). Triangles: Simulation of walking confined diffusion (Fig. 1). Circles: Simulation of free diffusion with the time-dependent diffusion coefficient  $D(t)$  given by eqn. (9). The slope of the dotted line is  $6D_m$ , where  $D_m$  is the microscopic diffusion coefficient. The slope of the dashed line is  $6D_M$ , where  $D_M$  is the macroscopic diffusion coefficient. Thin vertical line: crossover time  $\tau = a^2/(5D_m)$ . Inset: Theoretical curve in the log-log scale. The values of the parameters (see Section 3.1) are chosen typical for a sphere of diameter 90 nm diffusing in a 2% solution of PEG-2M.

obtained only numerically (see Section 3.1 for example results). This scaling may be similar to the that in the Rouse model (where  $\alpha$  changes from 1 through 1/2 again to 1) or in the reptation model (where  $\alpha$  changes from 1 through 1/2, 1/4, again to 1/2 and 1).<sup>25</sup>

### 2.4 Approximate propagator for diffusion with depletion layer

To obtain the approximate propagator  $p(\mathbf{r}', \mathbf{r}, t)$  for walking confined diffusion, we construct a process of free diffusion with the time-dependent diffusion coefficient  $D(t)$ , such that it has the same MSD (eqn. (7)) as the process of walking confined diffusion. We solve the modified diffusion equation with  $D(t)$ :

$$\frac{\partial}{\partial t} p(\mathbf{r}', \mathbf{r}, t) = D(t) \nabla^2 p(\mathbf{r}', \mathbf{r}, t), \quad (12)$$

and by separation of variables we get the time-dependent part of  $p(\mathbf{r}', \mathbf{r}, t)$ :

$$T(t) \sim e^{\int_0^t D(t') dt'} = e^{\frac{C}{2d} \langle \mathbf{r}^2(t) \rangle} \quad (13)$$

where  $C$  is an integration constant. By analogy to the case of a constant diffusion coefficient, the propagator can be, therefore, written as the Gaussian:

$$p(\mathbf{r}', \mathbf{r}, t) = \frac{1}{\left[ \frac{2\pi}{d} \langle \mathbf{r}^2(t) \rangle \right]^{d/2}} e^{-\frac{(\mathbf{r}' - \mathbf{r})^2}{\frac{2}{d} \langle \mathbf{r}^2(t) \rangle}}. \quad (14)$$

Substituting the MSD (eqn. (9)) and  $d = 3$ , we get the approximate propagator for walking confined diffusion:

$$p(\mathbf{r}', \mathbf{r}, t) = \frac{\exp\left[\frac{-(\mathbf{r}' - \mathbf{r})^2}{4D_M t + \frac{4}{5}a^2\left(1 - e^{-\frac{5D_M t}{a^2}}\right)}\right]}{\left[4\pi D_M t + \frac{4\pi}{5}a^2\left(1 - e^{-\frac{5D_M t}{a^2}}\right)\right]^{3/2}} \quad (15)$$

## 2.5 DLS and FCS autocorrelation functions for diffusion with depletion layer

The autocorrelation functions for DLS or FCS, calculated based on the propagator (eqn. (15)), contain the MSD for walking confined diffusion. For DLS, the autocorrelation function is the Fourier transform of eqn. (15).<sup>26</sup>

$$g(q, t) = e^{-\frac{1}{3}q^2\langle\mathbf{r}^2(t)\rangle} = Ae^{-\frac{1}{3}q^2\left[6D_M t + \frac{6}{5}a^2\left(1 - e^{-5D_M t/a^2}\right)\right]} \quad (16)$$

For FCS, the autocorrelation function<sup>27</sup> is the integral of eqn. (15) with the focal volume:

$$\begin{aligned} G(t) &= \left(1 + \frac{2}{3}\frac{\langle\mathbf{r}^2(t)\rangle}{w_{xy}^2}\right)^{-1} \left(1 + \frac{2}{3}\frac{\langle\mathbf{r}^2(t)\rangle}{\omega^2 w_{xy}^2}\right)^{-1/2} \\ &= \left(1 + \frac{2}{3}\frac{\left[6D_M t + \frac{6}{5}a^2\left(1 - e^{-5D_M t/a^2}\right)\right]}{w_{xy}^2}\right)^{-1} \\ &\quad \times \left(1 + \frac{2}{3}\frac{\left[6D_M t + \frac{6}{5}a^2\left(1 - e^{-5D_M t/a^2}\right)\right]}{\omega^2 w_{xy}^2}\right)^{-1/2}, \end{aligned} \quad (17)$$

where  $w_{xy}$  is the lateral size of the Gaussian volume,  $w_z$  is its transversal size, and  $\omega = w_{xy}/w_z$  is its elongation.

## 3 Predictions of experimental consequences of the depletion layer effect

### 3.1 Mean square displacement

In further considerations, we will use the values of parameters typical for a spherical probe of the radius  $R = 45$  nm diffusing in 0.4% solution of PEG-2M. We assume that the microscopic diffusion coefficient can be approximated by  $D_m = k_B T / (6\pi\eta_m R)$ , where  $k_B$  is the Boltzmann constant,  $T$  is temperature and  $\eta_m$  is the viscosity of the solvent. Based on the experimental data of Shimizu and Kenndler,<sup>16</sup> we take the macroscopic viscosity of the polymer solution  $\eta_M = 6.5 \eta_m$ , where the microscopic viscosity  $\eta_m = 1.002$  cP is the viscosity of water at the temperature  $T = 20$  °C. The radius of gyration of PEG-2M in water, as a function of the molecular mass  $M_p = 2 \times 10^6$ , is given<sup>17</sup> by  $R_g = 0.02M_p^{0.58} = 90.3$  nm. Assuming that PEG-2M can be described in the Gaussian limit, we use eqn. (2) to calculate the depletion layer thickness  $a = 77$  nm. The microscopic diffusion coefficient in water is  $D_m = 4.8 \times 10^{-12}$  m<sup>2</sup> s<sup>-1</sup>. The macroscopic diffusion coefficient of the probe diffusing

together with its depletion layer in the polymer solution is  $D_M = 2.7 \times 10^{-13}$  m<sup>2</sup> s<sup>-1</sup> (eqn. (1)), thus differing from  $D_m$  by one order of magnitude. The relaxation time, which marks the crossover between the micro- and macroscopic diffusion, is  $\tau = 0.25$  ms (eqn. (6)).

Fig. 2 shows the prediction of the dependence of MSD on time for the above values of parameters. The MSDs obtained from the simulation of walking confined diffusion (Fig. 1) and from the simulation of free diffusion with the time-dependent diffusion coefficient  $D(t)$ , given by eqn. (9), are both in perfect agreement with the theoretical MSD (eqn. (7)).

For  $t = \tau$ , the MSD scales as  $t^\alpha$  with  $\alpha \approx 0.62$ . For the time  $t \approx 1.1$  ms, in which the log-log plot of the MSD has the smallest slope,  $\alpha \approx 0.24$ . This scaling is similar to that of the motion of a monomer in the reptation model.<sup>25</sup>

Similar dependence of MSD on time was found in various experiments with diffusion in crowded environment. In single-molecule tracking experiments, it was detected as the effect of constrained diffusion of spherical probes in F-actin solutions,<sup>14,28–31</sup> spherical probes in fd-virus solutions,<sup>15</sup> carbon nanotubes in porous agarose networks,<sup>32</sup> promyelocytic leukemia nuclear bodies<sup>33</sup> and mRNA-protein complexes<sup>34</sup> in cell nucleus, and transmembrane MHC proteins on cell membrane.<sup>35</sup> In light scattering experiments, it was found in diffusion of spherical probes in PEO solutions<sup>20</sup> (diffusing wave spectroscopy (DWS) and quasielastic light scattering (QELS)), in F-actin solutions<sup>36</sup> (DWS), and in fd-virus solutions<sup>15</sup> (DLS). In FCS experiments, similar shapes of MSD curves were found in diffusion of probes in star polyisoprenes.<sup>37</sup> Some of those results were described in terms of hop diffusion (brownian motion constrained by immobile compartments)<sup>35</sup> or anomalous diffusion.<sup>14,15,28–30,32,33,36,37</sup>

### 3.2 Dynamic light scattering: Comparison between two-component diffusion and walking confined diffusion

In this section we compare our model of walking confined diffusion (eqn. (16)) with the typical model of two-component diffusion. Using the parameter values given by eqn. (2 – 1), we generated 100 artificial ‘data points’ (Fig. 4) from the theoretical formula for the DLS autocorrelation function (eqn. (16)) and made an attempt of a double-exponential fitting:

$$g_{\text{double,fit}}(q, t) = [A \exp(-q^2 D_1 t) + (1 - A) \exp(-q^2 D_2 t)]^2, \quad (18)$$

where  $q$  is the scattering vector length and  $D_1, D_2$  are coefficients of a two-component diffusion. The results (Table 1, Fig. 3) give different values of  $A, D_1$ , and  $D_2$  for different scattering angles. For  $q^2 \leq 10^{15}$  m<sup>-2</sup> the fits are good, however, for  $q^2$  above this value the fitting error of  $D_1$  increases excessively (but a single exponential can be fitted instead). Additionally, the double-exponential fitting was difficult for any  $q$ , because the fit converged to many different local minima.

We also made an attempt of a brute-force single exponential fitting for all  $q$ :

$$g_{\text{fit}}(q, t) = \exp(-2q^2 D_{\text{fit}} t), \quad (19)$$

Fig. 4 shows that the single exponential fits well for large scattering angles. The fitted diffusion coefficient  $D_{\text{fit}}$  increases

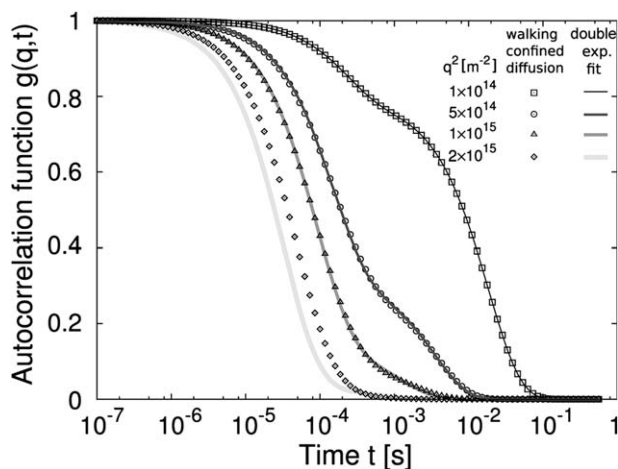


**Fig. 3** For small scattering angles in DLS, walking confined diffusion can be well fitted with two-component diffusion, however the diffusion coefficients  $D_1$ ,  $D_2$  are different for each  $q$  (Table 1). Symbols: Walking confined diffusion, artificial 'data points', generated using eqn. (16). Solid lines: Fitted autocorrelation function for two-component diffusion (eqn. (18)).

**Table 1** Fit of two-component diffusion to walking confined diffusion data points

$q^2$ [ $\text{m}^{-2}$ ]	$A$	$D_1$ [ $10^{-13} \text{ m}^2 \text{ s}^{-1}$ ]	$D_2$ [ $10^{-13} \text{ m}^2 \text{ s}^{-1}$ ]
$1 \times 10^{14}$	$0.88899 \pm 4 \times 10^{-5}$	$2.7021 \pm 0.0007$	$427.4 \pm 0.4$
$5 \times 10^{14}$	$0.567 \pm 0.001$	$2.85 \pm 0.03$	$108.0 \pm 0.5$
$1 \times 10^{15}$	$0.373 \pm 0.004$	$4.0 \pm 0.1$	$75.0 \pm 0.6$
$2 \times 10^{15}$	$0.163 \pm 0.009$	$3.3 \pm 0.6$	$57.0 \pm 0.6$

with  $q^2$  in a non-linear way (Fig. 5). For small scattering angles,  $D_{\text{fit}}$  tends to the macroscopic diffusion coefficient  $D_M$ , and for large scattering angles it tends to the microscopic diffusion coefficient  $D_m$ .

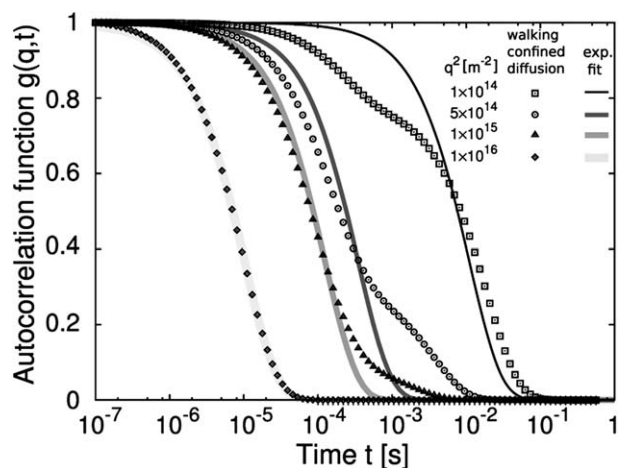


**Fig. 4** For large scattering angles in DLS, walking confined diffusion can be well fitted with one-component free diffusion, however the diffusion coefficients  $D_{\text{fit}}$  is different for each  $q$  (Fig. 5). Symbols: Walking confined diffusion, artificial 'data points', generated using eqn. (16). Solid lines: Fitted autocorrelation function for one-component free diffusion (eqn. (19)).

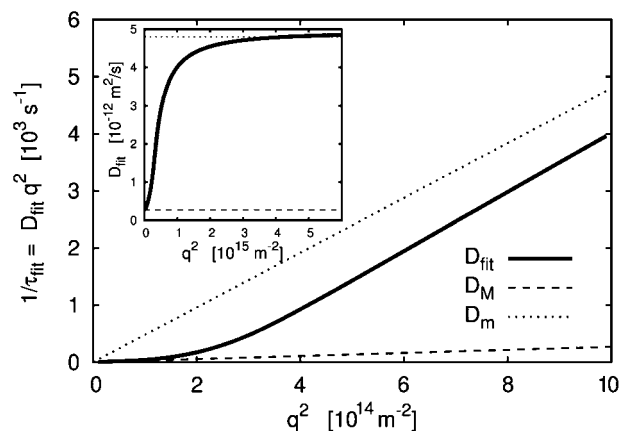


**Fig. 5** The fitted free diffusion coefficient  $D_{\text{fit}}$  depends on  $q^2$  when free-diffusion fitting (eqn. (19)) is attempted to the DLS 'data points' for walking confined diffusion. The 'data points' were generated from eqn. (16), as in Fig. 3 and 4. Main figure: Non-linear dependence of the fitted inverse relaxation time  $\tau_{\text{fit}}^{-1} = D_{\text{fit}}q^2$  on  $q^2$ . Inset: For small  $q^2$ ,  $D_{\text{fit}}$  tends to the macroscopic diffusion coefficient  $D_M$  (dashed line), and for large  $q^2$  it tends to the microscopic diffusion coefficient  $D_m$  (dotted line).

Similar shapes of autocorrelation functions were found in DLS experiments with diffusion of probes in entangled solutions of wormlike surfactant micelles<sup>38</sup> and diffusion of aggregates in solutions: ovalbumin<sup>39</sup> and DNA.<sup>40</sup> A non-linear dependence of the fitted inverse relaxation time  $\tau_{\text{fit}} = D_{\text{fit}}q^2$  on  $q^2$ , similar to that in the Fig. 5, was found in the experiments with diffusion of probes in ferrofluids.<sup>41</sup> Some of those experimental results were described in terms of anomalous diffusion.<sup>38,41</sup>

### 3.3 Fluorescence correlation spectroscopy

Using the parameter values given by eqn. (2 – 1), we generated artificial 'data points' from the theoretical formula for the FCS autocorrelation function (eqn. (17)), assuming  $w_{xy} = 180 \text{ nm}$  and  $\omega = 5$  as typical parameters of the FCS focal volume. We made an attempt of a brute-force fitting of the autocorrelation function for free diffusion (Fig. 6),

$$G_{\text{fit}}(t) = A \left( 1 + \frac{4D_{\text{fit}}t}{w_{xy}^2} \right)^{-1} \left( 1 + \frac{4D_{\text{fit}}t}{\omega^2 w_{xy}^2} \right)^{-1/2}, \quad (20)$$

to the artificial 'data points'. We tested linear and logarithmic binning (Fig. 6). Fitting yields the values of  $D_{\text{fit}} = 2.9 \times 10^{-13} \text{ m}^2 \text{ s}^{-1}$  for linear binning, and  $D_{\text{fit}} = 3.6 \times 10^{-13} \text{ m}^2 \text{ s}^{-1}$  for logarithmic binning, close to the macroscopic diffusion coefficient  $D_M$  because most of the 'data points' correspond to times  $t$  greater than the relaxation time  $\tau$ . Based on these results, we predict that the attempt of fitting the FCS autocorrelation function for free diffusion (eqn. (20)) to walking confined diffusion data allows one to detect the macroscopic diffusion only.

A similar effect was found in the experiment with globular protein in aqueous hyaluronan solution,<sup>42</sup> where FCS (with free diffusion assumed) was able to detect the macroscopic diffusion coefficient only, while other measurement methods detected the microscopic diffusion coefficient. Similar shapes of

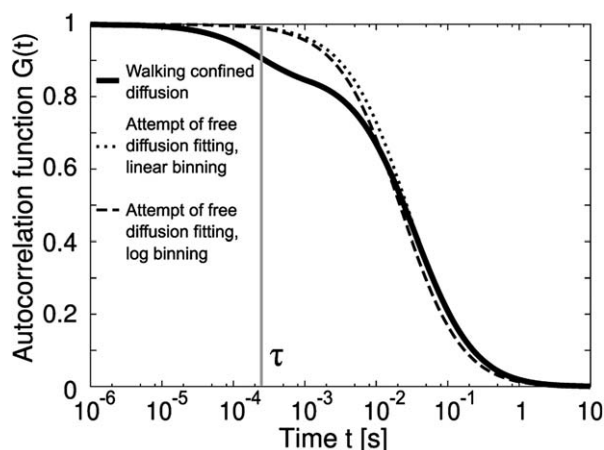


**Fig. 6** Only macroscopic diffusion can be detected when free-diffusion fitting (eqn. (20)) is attempted to the FCS ‘data points’ for walking confined diffusion. The ‘data points’ were generated from eqn. (17). The fitted diffusion coefficients for both linear (dotted line) and logarithmic binning (dashed line) are close to the macroscopic diffusion coefficient  $D_M$  because most of the ‘data points’ correspond to times  $t$  greater than the relaxation time  $\tau$ . To mimic linear binning,  $2 \times 10^6$  ‘data points’ were generated, starting from  $t = 10^{-6}$  s, every  $10^{-6}$  s. To mimic logarithmic binning, 170 ‘data points’ were generated starting from  $t = 10^{-6}$  s, incremented by the factor 1.1. For the sake of clarity of the figure, we present the ‘data points’ as connected by lines.

autocorrelation functions, found in experiments with in diffusion of probes in star polyisoprenes<sup>37</sup> and actin diffusion in living cells,<sup>43</sup> were theoretically described in terms of anomalous diffusion.

## 4 Comparison with experimental data

In this section we compare the model of walking confined diffusion to the existing experimental data.

### 4.1 Flexible polymer: Polyethylene oxide

The only published data for probes in the solution of flexible polymers that we found were the results of Dasgupta *et al.*<sup>20</sup> (Fig. 7). The MSD of polystyrene beads ( $R = 485$  nm) in a 4 wt% 900 kDa PEO solution was obtained from QELS and DWS measurements. The beads were much larger than the mesh size, which was a few nanometres. To date, no theory has been fitted to those results. Our formula for MSD (eqn. (7)) fits well for the time scales larger than  $10^{-1}$  s, while the crossover time  $\tau = 2$  s. The fit diverges for shorter times. The tracer diameter is 2 orders of magnitude larger than the mesh size  $\xi$  (Table 2). Therefore,  $D_m \sim D_M$ , which means that the experimental system does not fulfill the assumptions of our model (the diffusion of the probe and the diffusion of the depletion layer may be coupled).

### 4.2 Rigid polymers

Interestingly, we found that the model of walking confined diffusion fits very well to the diffusion of probes in the solutions of more rigid polymers (fd viruses and F-actin).

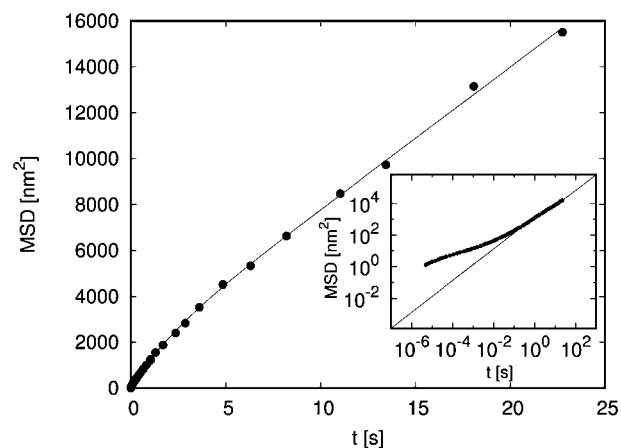


**Fig. 7** The model of walking confined diffusion fitted to the MSD of polystyrene beads ( $R = 485$  nm) in a 4 wt% was 900 kDa PEO solution (Dasgupta *et al.*<sup>20</sup>). The model fits well for the time scales larger than  $10^{-1}$  s (the crossover time is  $\tau = 2$  s). The fit diverges significantly for shorter times. Symbols: experimental data. Solid line: theory fitted (eqn. (7)).  $D_m = 120 \pm 6$  nm<sup>2</sup> s<sup>-1</sup>,  $D_M = 103 \pm 1$  nm<sup>2</sup> s<sup>-1</sup>,  $a = 36 \pm 1$  nm.

**Table 2** Depletion layer thickness predicted by our theory for existing experimental data, compared with the probe and mesh sizes

Reference	Probe radius $R$ [nm]	Depletion layer thickness $a$ / [nm]	Mesh size $\xi$ [nm]	$2R/\xi$	$a/\xi$
Dasgupta <i>et al.</i> <sup>20</sup>	485	36	$\sim 10^0$	$\sim 10^2$	$\sim 10^1$
Kang <i>et al.</i> <sup>15</sup>	500	77	391	2.6	0.2
	500	81	493	2.0	0.2
	500	117	683	1.5	0.2
Valentine <i>et al.</i> <sup>45</sup>	500	471	8000	0.1	0.06
	500	157	2000	0.5	0.2
	500	177	2000	0.5	0.2
Gardel <i>et al.</i> <sup>29</sup>	420	75	300	2.8	0.3
	320	92	300	2.1	0.3
	230	220	300	1.5	0.7
Gisler & Weitz <sup>36</sup>	1500	67	n/a	n/a	n/a
	260	26	n/a	n/a	n/a
Crocker <i>et al.</i> <sup>30</sup>	235	226	n/a	n/a	n/a

**4.2.1 Fd viruses.** Kang *et al.*<sup>15</sup> used DLS to measure the MSD of tracer spheres ( $R = 500$  nm) in the solution of rods of a well-defined length (fd-virus, contour length  $L = 880$  nm, thickness 6 nm). To date, no theory has been fitted to those results. We estimated the mesh size  $\xi$  assuming that at a given concentration the rods form a cubic lattice of the edge  $\xi$ . We used the data of Yodh *et al.*<sup>44</sup> to convert the fd-virus concentrations used by Kang *et al.*<sup>15</sup> into the number density. The overlap density would be 12 rods per volume  $L^3$ . Table 2 shows that the rods overlap ( $\xi < L$ ) and that the tracer diameter  $2R \sim \xi$ . Our theoretical formula for MSD (eqn. (7)) agrees very well with the experimental data (Fig. 8).

**4.2.2 F-actin.** Valentine *et al.*<sup>45</sup> used single-particle tracking to measure the MSD of PEG-coated tracers ( $R = 500$  nm) moving in the solution of F-actin and the actin-binding protein scruin that causes bundling of actin. The degree of bundling and bundle thickness depends on the actin to scruin ratio.<sup>46</sup>

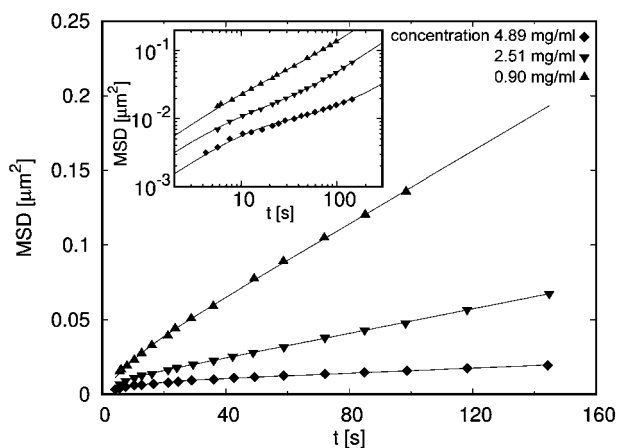


**Fig. 8** The model of walking confined diffusion describes very well the MSD of tracers ( $R = 500$  nm) in the solution of fd viruses (Kang *et al.*<sup>15</sup>). Symbols: experimental data for various fd-virus concentrations  $c$ . Solid line: theory fitted (eqn. (7)).  $\blacklozenge$ :  $c = 4.89$  mg ml<sup>-1</sup>,  $D_m = 125 \pm 7$  nm<sup>2</sup> s<sup>-1</sup>,  $D_M = 14.3 \pm 0.5$  nm<sup>2</sup> s<sup>-1</sup>,  $a = 77 \pm 1$  nm.  $\blacktriangledown$ :  $c = 2.51$  mg ml<sup>-1</sup>,  $D_m = 230 \pm 10$  nm<sup>2</sup> s<sup>-1</sup>,  $D_M = 68.6 \pm 0.4$  nm<sup>2</sup> s<sup>-1</sup>,  $a = 81 \pm 1$  nm.  $\blacktriangle$ :  $c = 0.90$  mg ml<sup>-1</sup>,  $D_m = 290 \pm 20$  nm<sup>2</sup> s<sup>-1</sup>,  $D_M = 204 \pm 3$  nm<sup>2</sup> s<sup>-1</sup>,  $a = 117 \pm 4$  nm.

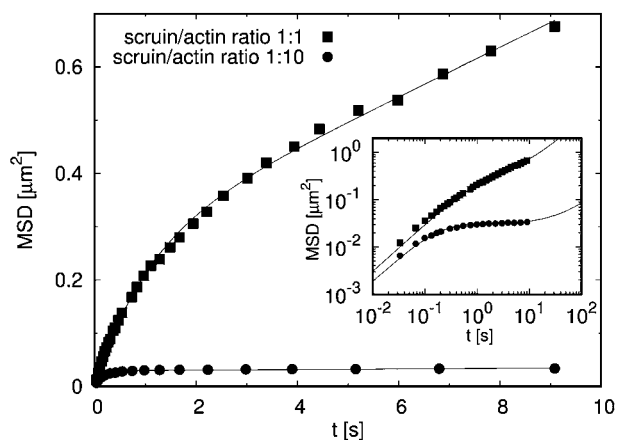


**Fig. 9** The model of walking confined diffusion describes well the MSD of PEG-coated tracers ( $R = 500$  nm) moving in the solution of F-actin and scruin (Valentine *et al.*<sup>45</sup>). The fits slightly diverge for times smaller than the crossover time  $\tau$ . Symbols: experimental data for varying actin/scruin ratios  $s$ . Solid line: theory fitted (eqn. (7)).  $\blacksquare$ :  $s = 1$ ,  $D_m = 43000 \pm 1000$  nm<sup>2</sup> s<sup>-1</sup>,  $D_M = 7700 \pm 300$  nm<sup>2</sup> s<sup>-1</sup>,  $a = 471 \pm 8$  nm,  $\tau = 1$  s.  $\bullet$ :  $s = 0.1$ ,  $D_m = 32000 \pm 1000$  nm<sup>2</sup> s<sup>-1</sup>,  $D_M = 90 \pm 20$  nm<sup>2</sup> s<sup>-1</sup>,  $a = 157 \pm 1$  nm,  $\tau = 0.15$  s.

The concentration of actin was  $0.5$  mg ml<sup>-1</sup>, and the amount of scruin was varied. To date, no theory has been fitted to those results. We used the data of Shin *et al.*<sup>46</sup> to estimate  $\xi$  for various actin:scruin ratios. Table 2 shows that the tracer diameter  $2R \sim \xi$ . Our theoretical formula for MSD (eqn. (7)) agrees well with the experimental data (Fig. 9), although the fit slightly diverges for times smaller than the crossover time  $\tau$ .

We also obtained relatively good fits to the data of Gardel *et al.*<sup>29</sup> (Fig. 10). The MSD of tracers ( $R = 420$  nm,  $320$  nm, and  $230$  nm) in the solution  $0.9$  mg ml<sup>-1</sup> of F-actin was measured by single molecule tracking. To date, no theory has been fitted to those results. Our theoretical formula for MSD (eqn. (7)) fits

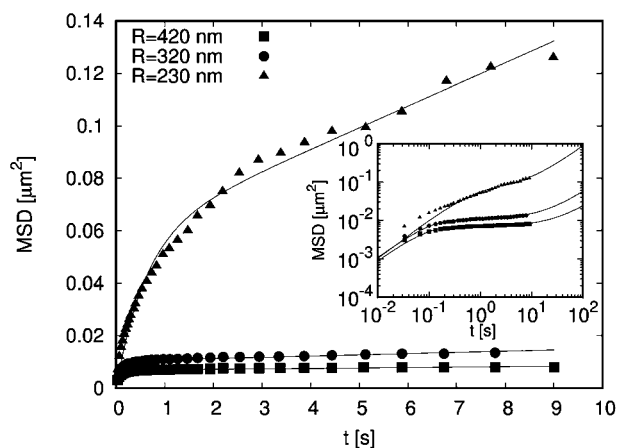


**Fig. 10** The model of walking confined diffusion describes relatively well the MSD of tracers in the solution  $0.9$  mg ml<sup>-1</sup> of F-actin (Gardel *et al.*<sup>29</sup>). The fits are quite good for larger tracers ( $R = 420$  nm and  $320$  nm), although they slightly diverge for times smaller than the crossover time  $\tau$ . For  $R = 230$  nm, the divergence is significant. Symbols: experimental data for varying tracer radii  $R$ . Solid line: theory fitted (eqn. (7)).  $\blacksquare$ :  $R = 420$  nm,  $D_m = 15800 \pm 800$  nm<sup>2</sup> s<sup>-1</sup>,  $D_M = 29 \pm 3$  nm<sup>2</sup> s<sup>-1</sup>,  $a = 75.1 \pm 0.4$  nm,  $\tau = 0.07$  s.  $\bullet$ :  $R = 320$  nm,  $D_m = 19000 \pm 1000$  nm<sup>2</sup> s<sup>-1</sup>,  $D_M = 79 \pm 6$  nm<sup>2</sup> s<sup>-1</sup>,  $a = 92.6 \pm 0.5$  nm,  $\tau = 0.09$  s.  $\blacktriangle$ :  $R = 230$  nm,  $D_m = 16000 \pm 1000$  nm<sup>2</sup> s<sup>-1</sup>,  $D_M = 1380 \pm 90$  nm<sup>2</sup> s<sup>-1</sup>,  $a = 220 \pm 5$  nm,  $\tau = 0.6$  s.

quite well for larger tracers ( $2R/\xi \approx 2.8$  and  $2R/\xi \approx 2.1$ , Table 2), however it slightly diverges for times smaller than the crossover time  $\tau$ . For  $2R/\xi \approx 1.5$ , the divergence is significant.

However, the MSD data for F-actin should be studied with caution because the solutions may not be well controlled. The F-actin exhibits a polydisperse length distribution.<sup>15</sup>

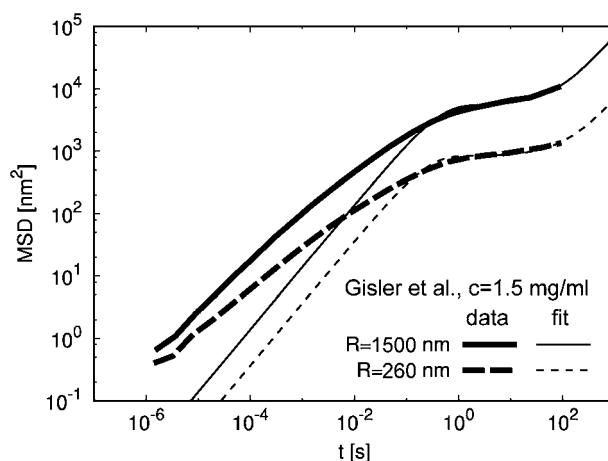


**Fig. 11** The experimental data of Gisler & Weitz<sup>36</sup> are inconsistent. The MSD of probes in a  $1.5$  mg ml<sup>-1</sup> F-actin solution was measured using DLS. The probes of  $R = 1500$  nm diffuse one order of magnitude faster than the probes of  $R = 260$  nm. This unphysical result may be due to a wrong normalization of the DLS autocorrelation function. The fits of the walking confined diffusion model strongly diverge in the time scales shorter than the crossover time  $\tau$ . Thick lines: experimental data. Thin lines: theory fitted (eqn. (7)). For  $R = 1500$  nm:  $D_m = 2300 \pm 300$  nm<sup>2</sup> s<sup>-1</sup>,  $D_M = 10.9 \pm 0.7$  nm<sup>2</sup> s<sup>-1</sup>,  $a = 67 \pm 1$  nm,  $\tau = 0.4$  s. For  $R = 260$  nm:  $D_m = 600 \pm 80$  nm<sup>2</sup> s<sup>-1</sup>,  $D_M = 1.0 \pm 0.1$  nm<sup>2</sup> s<sup>-1</sup>,  $a = 26.3 \pm 0.5$  nm,  $\tau = 0.2$  s.

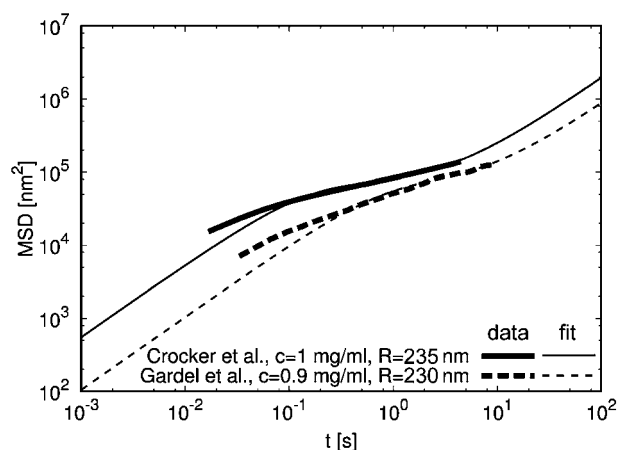


**Fig. 12** The experimental data of Crocker *et al.*<sup>30</sup> are inconsistent with the data of Gardel *et al.*<sup>29</sup> (single-particle tracking was used in both experiments): Larger probes diffuse slightly faster in a higher concentration of F-actin solution than smaller probes in a lower concentration. The fits of the walking confined diffusion model strongly diverge in the time scales shorter than the crossover time  $\tau$ . Thick lines: experimental data. Thin lines: theory fitted (eqn. (7)). For Crocker *et al.*,  $R = 235$  nm,  $c = 1$  mg ml<sup>-1</sup>:  $D_m = 89000 \pm 60000$  nm<sup>2</sup> s<sup>-1</sup>,  $D_M = 3100 \pm 100$  nm<sup>2</sup> s<sup>-1</sup>,  $a = 226 \pm 3$  nm,  $\tau = 0.1$  s. For Gardel *et al.*,  $R = 230$  nm ( $al\xi \approx 0.6$ ),  $D_m = 16000 \pm 1000$  nm<sup>2</sup> s<sup>-1</sup>,  $D_M = 1380 \pm 90$  nm<sup>2</sup> s<sup>-1</sup>,  $a = 220 \pm 5$  nm,  $\tau = 0.6$  s (same as in Fig. 10).

Uncontrolled bundling and continuous polymerization and depolymerization of the filaments may also occur.<sup>15</sup> We have found papers in which the data are inconsistent: a) DLS (Fig. 11): In Gislis & Weitz<sup>36</sup> (1.5 mg ml<sup>-1</sup> F-actin solution), larger probes ( $R = 1500$  nm) diffuse one order of magnitude faster than smaller probes ( $R = 260$  nm). This unphysical result may be an artifact of wrong normalization of the DLS autocorrelation function. b) Single-particle tracking (Fig. 12): In Crocker *et al.*,<sup>30</sup> larger probes in a higher F-actin concentration ( $R = 235$  nm,  $c = 1$  mg ml<sup>-1</sup>) diffuse faster than slightly smaller probes in a lower concentration, measured by Gardel *et al.*<sup>29</sup> ( $R = 230$  nm,  $c = 0.9$  mg ml<sup>-1</sup>).

In the above examples, a) and b), the theoretical MSDs strongly diverge in the time scales shorter than the crossover time  $\tau$ . We hypothesize that this divergence is due to polydispersity of the solution. The presence of short molecules 'softens' the boundary of the depletion layer, while our model assumes an ideally reflecting boundary. On the other hand, the examples of rigid polymers of a well-defined length (Fig. 8, 9) fit well to our model probably because the rods form a rigid cage around the probe, such that the assumption of reflecting boundary conditions is fulfilled.

## 5 Conclusions

Anomalous transport in crowded environments, such as the interior of living cells, increasingly attracts the attention of researchers.<sup>47,48</sup> Recently, elaborate theoretical tools have been developed to understand the non-linear behavior of MSD<sup>49</sup> in systems with anomalous diffusion and to predict the FCS autocorrelation functions<sup>50</sup> for that type of motion. In this paper, we show that the effects characteristic of anomalous diffusion may

occur due to the diffusion with depletion layer, for which the simplest theoretical description is walking confined diffusion, *i.e.* the sum of two independent motions: i) fast confined diffusion of the probe within a spherical domain filled with solvent (microscopic diffusion), and ii) slow free diffusion of the domain with the probe through the polymer solution (macroscopic diffusion). We derive the formula that describes the non-linear behavior of MSD in time for walking confined diffusion. Using that formula, we construct the approximate propagator and the corresponding autocorrelation functions for DLS and FCS.

We theoretically predict the experimental consequences of the existence of depletion using the literature data for PEG. We show the non-linear behavior of MSD and determine the crossover time between the microscopic and macroscopic diffusion, as well as the anomalous exponents corresponding to different time scales. Using the theoretical formulas for the autocorrelation functions, we generate artificial 'data points' that mimic the DLS and FCS experiments. For DLS, we test the fitting the two-component diffusion or single-component free diffusion autocorrelation functions to walking confined diffusion data. We predict that such attempts will result in the fitted diffusion coefficients depending on the scattering angle. For FCS, we predict that only macroscopic diffusion can be detected when free-diffusion fitting is attempted to walking confined diffusion data.

We compare our model of walking confined diffusion to existing experimental data for solutions of flexible (PEO, and rigid polymers (fd-viruses and F-actin). We have found only one suitable study of flexible polymers and our model fits well to those data in intermediate to long time scales. On the other hand, the model of walking confined diffusion fits very well to the data for rigid polymers of a well-defined length. Some data for F-actin may be affected by its polydispersity. We have also found inconsistencies between some data for F-actin, which suggests that the experiments may have been carried out in poorly controlled solutions. The comparison shows that there is a need for new, well-controlled experiments for F-actin and flexible polymers (such as PEO or PEG).

The eqn. (16) and (17) derived here are ready to be fitted to DLS and FCS experimental data for probes diffusing in polymer solutions.

## Acknowledgements

The project was operated within the Foundation for Polish Science TEAM Program cofinanced by the European Union European Regional Development Fund (TEAM/2008-2/2) and supported by the Polish Ministry of Science and Higher Education grant Iuventus Plus no. IP2010 028870.

## References

- 1 S. Asakura and F. Oosawa, *J. Polym. Sci.*, 1958, **33**, 183–192.
- 2 A. Vrij, *Pure Appl. Chem.*, 1976, **48**, 471–483.
- 3 P. de Gennes, *Scaling concepts in polymer physics*, Cornell Univ Pr, 1979.
- 4 G. Fleer, A. Skvortsov and R. Tuinier, *Macromolecules*, 2003, **36**, 7857–7872.
- 5 G. Phillies, *Macromolecules*, 1995, **28**, 8198–8208.
- 6 G. Phillies, *Macromolecules*, 1986, **19**, 2367–2376.

- 7 R. Hołyst, A. Bielejewska, J. Szymański, A. Wilk, A. Patkowski, J. Gapiński, A. Żywociński, T. Kalwarczyk, E. Kalwarczyk and M. Tabaka, *Phys. Chem. Chem. Phys.*, 2009, **11**, 9025–9032.
- 8 R. Tuinier, J. Dhont and T. Fan, *Europhys. Lett.*, 2006, **75**, 929.
- 9 T. Fan, J. Dhont and R. Tuinier, *Phys. Rev. E: Stat., Nonlinear, Soft Matter Phys.*, 2007, **75**, 11803.
- 10 R. Tuinier and T. Fan, *Soft Matter*, 2008, **4**, 254–257.
- 11 F. Daumas, N. Destainville, C. Millot, A. Lopez, D. Dean and L. Salomé, *Biophys. J.*, 2003, **84**, 356–366.
- 12 T. Fan, B. Xie and R. Tuinier, *Phys. Rev. E: Stat., Nonlinear, Soft Matter Phys.*, 2007, **76**, 51405.
- 13 T. Mason and D. Weitz, *Phys. Rev. Lett.*, 1995, **74**, 1250–1253.
- 14 I. Wong, M. Gardel, D. Reichman, E. Weeks, M. Valentine, A. Bausch and D. Weitz, *Phys. Rev. Lett.*, 2004, **92**, 178101.
- 15 K. Kang, J. Gapinski, M. Lettinga, J. Buitenhuis, G. Meier, M. Ratajczyk, J. Dhont and A. Patkowski, *J. Chem. Phys.*, 2005, **122**, 044905.
- 16 T. Shimizu and E. Kenndler, *Electrophoresis*, 1999, **20**, 3364–3372.
- 17 K. Devanand and J. Selser, *Macromolecules*, 1991, **24**, 5943–5947.
- 18 R. Tuinier, *Eur. Phys. J. E*, 2003, **10**, 123–128.
- 19 J. Wu and K. Berland, *Biophys. J.*, 2008, **95**, 2049–2052.
- 20 B. Dasgupta, S. Tee, J. Crocker, B. Frisken and D. Weitz, *Phys. Rev. E: Stat. Phys., Plasmas, Fluids, Relat. Interdiscip. Top.*, 2002, **65**, 51505.
- 21 P. Hassan, K. Bhattacharya, S. Kulshreshtha and S. Raghavan, *J. Phys. Chem. B*, 2005, **109**, 8744–8748.
- 22 R. Shusterman, S. Alon, T. Gavrinov and O. Krichevsky, *Phys. Rev. Lett.*, 2004, **92**, 48303.
- 23 A. Krall and D. Weitz, *Phys. Rev. Lett.*, 1998, **80**, 778–781.
- 24 T. Bickel, *Phys. A*, 2007, **377**, 24–32.
- 25 K. Kremer, in *Computational Soft Matter: From Synthetic Polymers to Proteins, Lecture Notes*, ed. N. Attig, K. Binder, H. Grubmüller and K. Kremer, John von Neumann Institute for Computing, Jülich, 2004, vol. 23, ch. Entangled polymers: From universal aspects to structure property relations, pp. 141–168.
- 26 B. Berne and R. Pecora, *Dynamic light scattering: with applications to chemistry, biology, and physics*, Dover Pubns, 2000.
- 27 R. Shusterman, T. Gavrinov and O. Krichevsky, *Phys. Rev. Lett.*, 2008, **100**, 98102.
- 28 J. Liu, M. Gardel, K. Kroy, E. Frey, B. Hoffman, J. Crocker, A. Bausch and D. Weitz, *Phys. Rev. Lett.*, 2006, **96**, 118104.
- 29 M. Gardel, M. Valentine, J. Crocker, A. Bausch and D. Weitz, *Phys. Rev. Lett.*, 2003, **91**, 158302.
- 30 J. Crocker, M. Valentine, E. Weeks, T. Gisler, P. Kaplan, A. Yodh and D. Weitz, *Phys. Rev. Lett.*, 2000, **85**, 888–891.
- 31 Y. Tseng and D. Wirtz, *Biophys. J.*, 2001, **81**, 1643–1656.
- 32 N. Fakhri, F. MacKintosh, B. Lounis, L. Cognet and M. Pasquali, *Science*, 2010, **330**, 1804.
- 33 Y. Chen, C. Kappel, J. Beaudouin, R. Eils and D. Spector, *Mol. Biol. Cell*, 2008, **19**, 3147.
- 34 Y. Shav-Tal, X. Darzacq, S. Shenoy, D. Fusco, S. Janicki, D. Spector and R. Singer, *Science*, 2004, **304**, 1797.
- 35 Y. Umemura, M. Vrljic, S. Nishimura, T. Fujiwara, K. Suzuki and A. Kusumi, *Biophys. J.*, 2008, **95**, 435–450.
- 36 T. Gisler and D. Weitz, *Phys. Rev. Lett.*, 1999, **82**, 1606–1609.
- 37 T. Cherdhirankorn, G. Floudas, H. Butt and K. Koynov, *Macromolecules*, 2009, **42**, 9183–9189.
- 38 A. Shukla, R. Fuchs and H. Rehage, *Langmuir*, 2006, **22**, 3000–3006.
- 39 M. Weijers, R. Visschers and T. Nicolai, *Macromolecules*, 2002, **35**, 4753–4762.
- 40 L. Spindler, M. Rigler, I. Drevenšek-Olenik, N. Hessari and M. da Silva, *J. Nucleic Acids*, 2010, **2010**, year.
- 41 A. Mertelj, L. Cmok and M. Čopič, *Phys. Rev. E: Stat., Nonlinear, Soft Matter Phys.*, 2009, **79**, 41402.
- 42 A. Masuda, K. Ushida, G. Nishimura, M. Kinjo, M. Tamura, H. Koshino, K. Yamashita and T. Kluge, *J. Chem. Phys.*, 2004, **121**, 10787.
- 43 H. Engelke, D. Heinrich and J. Rädler, *Phys. Biol.*, 2010, **7**, 046014.
- 44 A. Yodh, K. Lin, J. Crocker, A. Dinsmore, R. Verma and P. Kaplan, *Philos. Trans. R. Soc. London, Ser. A*, 2001, **359**, 921.
- 45 M. Valentine, Z. Perlman, M. Gardel, J. Shin, P. Matsudaira, T. Mitchison and D. Weitz, *Biophys. J.*, 2004, **86**, 4004–4014.
- 46 J. Shin, M. Gardel, L. Mahadevan, P. Matsudaira and D. Weitz, *Proc. Natl. Acad. Sci. U. S. A.*, 2004, **101**, 9636.
- 47 J. Mika and B. Poolman, *Curr. Opin. Biotechnol.*, 2011, **22**, 117–126.
- 48 N. Malchus and M. Weiss, *J. Fluoresc.*, 2010, **20**, 19–26.
- 49 H. Sun, W. Chen, H. Sheng and Y. Chen, *Phys. Lett. A*, 2010, **374**, 906–910.
- 50 F. Höfling, K. Bamberg and T. Franosch, *Soft Matter*, 2011, **7**, 1358–1363.